Bioorganic & Medicinal Chemistry Letters 20 (2010) 5607–5612

Contents lists available at ScienceDirect

Bioorganic & Medicinal Chemistry Letters

journal homepage: www.elsevier.com/locate/bmcl

# Discovery of pyrrolopyrimidine inhibitors of Akt

James F. Blake [a,*], Nicholas C. Kallan [a], Dengming Xiao [a], Rui Xu [a], Josef R. Bencsik [a], Nicholas J. Skelton [b], Keith L. Spencer [a], Ian S. Mitchell [a], Richard D. Woessner [a], Susan L. Gloor [a], Tyler Risom [a], Stefan D. Gross [a], Matthew Martinson [a], Tony H. Morales [a], Guy P. A. Vigers [a], Barbara J. Brandhuber [a]

[a] Array BioPharma Inc., 3200 Walnut Street, Boulder, CO 80301, USA
[b] Genentech Inc., 1 DNA Way, South San Francisco, CA 94080-4990, USA

ARTICLE INFO

*Article history:*
Received 30 June 2010
Revised 9 August 2010
Accepted 11 August 2010
Available online 13 August 2010

*Keyword:*
Akt kinase inhibitors

ABSTRACT

The discovery and optimization of a series of pyrrolopyrimidine based protein kinase B (Pkb/Akt) inhibitors discovered via HTS and structure based drug design is reported. The compounds demonstrate potent inhibition of all three Akt isoforms and knockdown of phospho-PRAS40 levels in LNCaP cells and tumor xenografts.



Protein kinase B (Pkb/Akt) is a serine–threonine kinase and downstream target for phosphatidylinositol 3-kinase (PI3K) that plays a central role in the regulation of cell survival and proliferation.[1] Constitutive activation and overexpression of Akt has been identified in a wide variety of human tumors, including breast, prostate, and ovarian carcinomas.[2] Additionally, loss of PTEN activity in a large number of tumors further contributes to the attractiveness of inhibiting Akt activity as a novel therapeutic approach to cancer treatment.[3] Akt comprises three isoforms (Akt1, Akt2, and Akt3) that share significant sequence identity while possessing disparate functions.[4] Knockout data using Akt shRNA suggests that maximum efficacy in tumor-bearing nude mice would be achieved by inhibiting all three isoforms.[5]

We describe the discovery and optimization of a series of pan Akt inhibitors that were discovered via combinatorial library synthesis, high throughput screening (HTS), and structure based drug design. Originally, compound **1** (Fig. 1) was synthesized as part of a combinatorial library that targeted the ATP cleft of kinases. HTS screening identified **1** as a hit against Akt1 with an $IC_{50}$ = 2.1 μM.[6] Synthesis of the individual enantiomers with (*R*)-(**2**), and (*S*)-stereochemistry (**3**) showed a marked difference in potency with Akt1 $IC_{50}$s of 884 nM and >85 μM, respectively.

While no X-ray structures of Akt1 were available at the outset of our efforts, several X-ray structures of Akt2 and PKA kinases were known.[7] Given the high identity among the kinase domains of Akt1/2/3, use of the X-ray structure of Akt2 for our early optimization efforts was a viable strategy.

Docking of compounds **2** and **3** suggested that the former could more easily form better interactions with Glu236, Glu279, and the hydrophobic residues present in the P-loop (Fig. 2).[8] In this model the quinazoline ring occupies the hydrophobic cavity near the hinge region and accepts a hydrogen bond from the backbone NH of Ala232. Based on the docked structure of **2**, we prepared a series of substituted benzyl analogs to probe the SAR of the nascent hit (Table 1). Small hydrophobic substitution proved to afford the largest potency increases. Replacement of the phenyl ring with 1-napthyl (**15**) resulted in significantly lower potency versus Akt1 (3.2 μM), as did the incorporation of 2- (**20**) or 3-pyridyl (**21**), 43.1 μM and 7.1 μM, respectively. Neither the secondary (**22**, 3.2 μM), nor tertiary amine (**23**, 7.7 μM) of **2**, proved to be potent inhibitors of Akt1, presumably owing to loss of interaction with the two glutamate residues. From this evaluation, **4** emerged as our initial lead for further optimization efforts.

In vitro cellular potency of **4** was assessed by measurement of phospho-PRAS40 levels in the LNCaP cell line (cell $IC_{50}$ = 1.5 μM).[9] Additionally, **4** was shown to possess excellent aqueous solubility of 3.6 mg/mL (at pH 7.4 via shake flask method).

Initial SAR around the quinazoline ring probed for possible positions that would allow for additional diversification (Table 2).

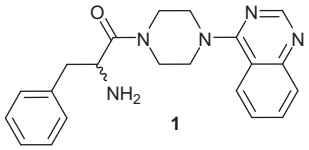


1

**Figure 1.** Combinatorial library HTS hit.

* Corresponding author. Tel.: +1 303 386 1262.
*E-mail address:* jblake@arraybiopharma.com (J.F. Blake).

0960-894X/$ - see front matter © 2010 Elsevier Ltd. All rights reserved.
doi:10.1016/j.bmcl.2010.08.053

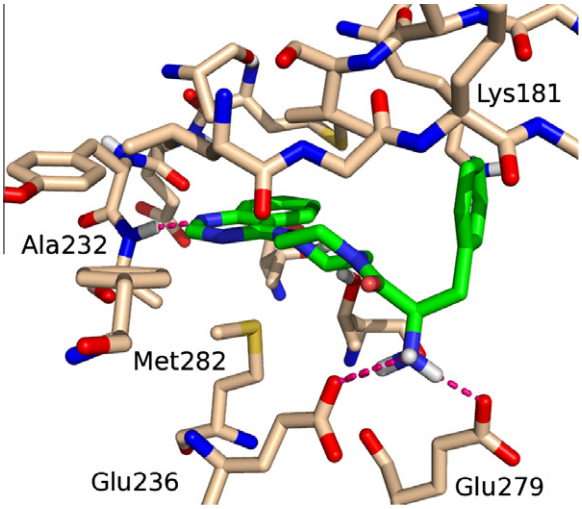


**Figure 2.** Compound **2** docked into the X-ray structure of Akt2 (PDB code: 1O6K).

**Table 1**
Akt kinase inhibition

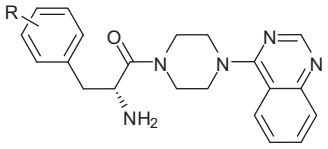

| Compound | R | Akt1 inhibition $IC_{50}$[a] (nM) | Akt2 inhibition $IC_{50}$[a] (nM) | Akt3 inhibition $IC_{50}$[a] (nM) |
|---|---|---|---|---|
| **2** | H | 884 ± 238 | 8362 ± 5146 | 8410 ± 1354 |
| **4** | 4-Cl | 20 ± 6 | 118 ± 47 | 179 ± 29 |
| **5** | 4-CN | 284 ± 112 | 4371 ± 2649 | 2718 ± 334 |
| **6** | 4-F | 118 ± 20 | 1288 ± 431 | 1122 ± 275 |
| **7** | 4-$OCH_3$ | 150 ± 40 | 1485 ± 569 | 2056 ± 398 |
| **8** | 4-$CH_3$ | 74 ± 34 | 630 ± 159 | 754 ± 84 |
| **9** | 4-Br | 30 ± 5 | 279 ± 60 | 363 ± 92 |
| **10** | 2-Cl | 2346 ± 1040 | 26,500 ± 9339 | 25,110 ± 4174 |
| **11** | 3-Cl | 595 ± 238 | 5586 ± 2345 | 6079 ± 1589 |
| **12** | 2-,4-diCl | 142 ± 36 | 1067 ± 359 | 1464 ± 62 |
| **13** | 3-,4-diCl | 51 ± 17 | 433 ± 85 | 485 ± 63 |
| **14** | 3-,4-diF | 81 ± 7 | 872 ± 305 | 666 ± 33 |
| **16** | 4-$CF_3$ | 95 ± 34 | 707 ± 178 | 746 ± 65 |
| **17** | 4-Phenyl | 2883 ± 781 | 37,826 ± 13,890 | 13,916 ± 1527 |
| **18** | 3-,5-diF | 690 ± 263 | 5027 ± 1389 | 6073 ± 1262 |
| **19** | 3-,4-$OCH_3$ | 838 ± 428 | 4951 ± 1362 | 5769 ± 739 |

[a] Values are means of three or more experiments, standard deviation is given.

Although several of the quinazoline ring substitutions were tolerated, none improved the potency, which led us to explore alternate hinge binding cores while maintaining the 4-Cl benzyl amino acid of **4**.

A number of the quinazoline replacements showed excellent potency (Table 3), and introduction of a hydrogen bond donor for interaction with the carbonyl of Glu228 at the hinge resulted in a significant potency boost (e.g., **40** and **44**).

Substitution of methyl at C5 (**46**) on the pyrrolopyrimidine core resulted in a substantial boost in Akt1 potency, with an $IC_{50}$ of ca. 1 nM (Table 4). Subsequent substitution of ethyl (**47**), cyclopropyl (**48**), and Cl (**49**) produced compounds with similar levels of potency relative to the methyl substituted core. Methyl substitution at C6 led to decreased potency (Akt1 $IC_{50}$ = 52 nM; **60**) as did the 5-,6-dimethyl analog (Akt1 $IC_{50}$ = 21 nM; **61**).

**Table 2**
Quinazoline ring SAR

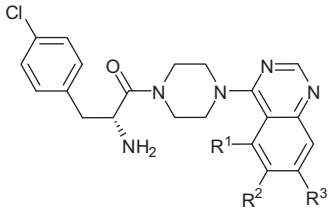

| Compound | $R^1$ | $R^2$ | $R^3$ | Akt1 inhibition $IC_{50}$[a] (nM) |
|---|---|---|---|---|
| **24** | H | H | $CH_3$ | 3203 ± 1348 |
| **25** | H | H | F | 30 ± 12 |
| **26** | $CH_3$ | H | H | 100 ± 59 |
| **27** | H | $CH_3$ | H | 54 ± 21 |
| **28** | H | 4-Pyrazole | H | 80 ± 43 |
| **29** | H | $NH_2$ | H | 43 ± 22 |
| **30** | H | $NHCH_3$ | H | 98 ± 19 |
| **31** | H | $N(CH_3)_2$ | H | 536 ± 201 |
| **32** | H | *N*-Acetamide | H | 868 ± 438 |
| **33** | H | *N*-Methylsulfonamide | H | 174 ± 72 |
| **34** | H | Phenyl | H | 809 ± 215 |
| **35** | H | *t*-Butyl | H | 1460 ± 775 |

[a] Values are means of three or more experiments, standard deviation is given.

The influence of amine chain length on potency was probed. β-amino amides (**50**–**53**) were nearly as potent as the shorter α-amino amides. Moreover, the longer β-amino amide side chain afforded the possibility of maintaining the same overall relationship between the aromatic ring and amine position via deletion of the methylene linker of the former. Thus, the 4-Cl phenyl β-amino acid, coupled with the pyrrolopyrimidine core proved to be quite potent (e.g., **56**, Table 4). As in the quinazoline series, the amine (*S*)-stereoisomer proved much less potent (**57**). In general, we found that primary α-amino amides tended to have cellular potency similar to the β-amino amides (e.g., **46** and **56**, cell $IC_{50}$ = 38 nM and 138 nM, respectively). For all of these analogs, the Akt2 and Akt3 potencies followed the same trends albeit with potencies ca. 5–10 fold lower than versus Akt1.

Access to the 5-methyl pyrrolopyrimidines originated from readily available pyrrolopyrimidine **62** as shown in Scheme 1. Treatment of **62** with *N*-bromosuccinimide gave clean bromination at the 5-position. Subsequent nitrogen protection as the phenyl sulfonamide and incorporation of the Boc protected piperazine via $S_NAr$ gave **63** in good overall yield. Conversion of the bromide to the methyl was smoothly mediated under Pd catalyzed conditions, which following acid promoted Boc deprotection, afforded **64** as the di-HCl salt. Synthesis of the pool of (*R*) α-amino acids used to prepare compounds **2**–**45** was achieved using a chiral hydrogenation route as outlined in Scheme 2.

Formation of the key amino acrylate by treatment of the appropriate aldehyde under Horner–Wadsworth–Emmons conditions led exclusively to the *Z* regioisomer **65** in good yield. Asymmetric reduction using catalytic Rh-(*R*,*R*)-DuPhos under 40 psi hydrogen, followed by subsequent ester hydrolysis provided the desired (*R*) α-amino acid in excellent yield and >95% ee, as determined by chiral HPLC.

The β-amino acids originated from readily available phenyl acetate esters (Scheme 3). Hydroxymethylation of the ester by treatment with paraformaldehyde and NaOMe, followed by activation to the mesylate and concomitant β-elimination gave acrylate **66**.

Introduction of the amine by Michael addition followed by successive amine protection as the *t*-butyl carbamate and ester

**Table 3**
Alternative hinge binding motifs

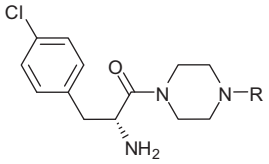

| Compound | R | Akt1 inhibition $IC_{50}$[a] (nM) | Compound | R | Akt1 inhibition $IC_{50}$[a] (nM) |
|---|---|---|---|---|---|
| **36** | 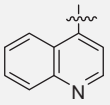 | 46 ± 11 | **41** | 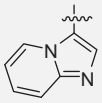 | 8122 ± 1410 |
| **37** | 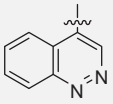 | 21,233 ± 9368 | **42** | 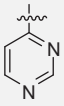 | 22,920 ± 7402 |
| **38** | 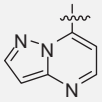 | 3321 ± 337 | **43** | 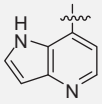 | 2048 ± 851 |
| **39** | 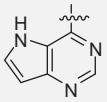 | 114 ± 83 | **44** | 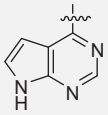 | 5 ± 2 |
| **40** | 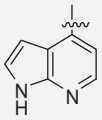 | 8 ± 4 | **45** | 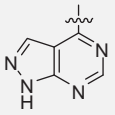 | 104 ± 33 |

[a] Values are means of three or more experiments, standard deviation is given.

**Table 4**
Pyrrolopyrimidine SAR

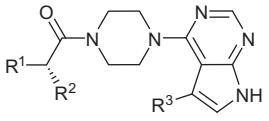

| Compound | $R^1$ | $R^2$ | $R^3$ | Akt1 inhibition $IC_{50}$[a] (nM) |
|---|---|---|---|---|
| **46** | 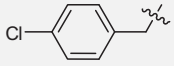 | $NH_2$ | $CH_3$ | 1 ± 0 |
| **47** | | $NH_2$ | Ethyl | 2 ± 1 |
| **48** | | $NH_2$ | *cyclo*Pr | 2 ± 1 |
| **49** | | $NH_2$ | Cl | 1 ± 0 |
| **50** | | $CH_2NH_2$ | H | 5 ± 2 |
| **51** | | $CH_2NH_2$ | $CH_3$ | 2 ± 0 |
| **52** | | $CH_2NHCH_3$ | H | 18 ± 5 |
| **53** | | $CH_2N(CH_3)_2$ | H | 88 ± 23 |
| **54** | 4-F benzyl | $NH_2$ | $CH_3$ | 3 ± 2 |
| **55** | 2-(2,3)Dihydroindene | $NH_2$ | $CH_3$ | 30 ± 7 |
| **56** | 4-Cl phenyl | $CH_2NH_2$ | H | 2 ± 1 |
| **57** | | (*S*)-$CH_2NH_2$ | H | 63 ± 32 |
| **58** | 3-,4-diCl phenyl | $CH_2NH_2$ | Cl | 2 ± 0 |
| **59** | 4-iPr benzyl | $CH_2NH_2$ | H | 604 ± 319 |

[a] Values are means of three or more experiments, standard deviation is given.

hydrolysis gave the racemic β-amino acid **67** in excellent overall yield. The chiral amino acid was obtained from separation of the racemate via SFC. With the requisite amino acid and core in hand, coupling was carried out using the conditions illustrated in Scheme 4. Treatment of the amine **68** with Hünig's base, HBTU and the appropriate amino acid gave **69** in excellent yield. Subsequent hydrolysis of the phenyl sulfonamide and Boc deprotection afforded the desired compound **70** as the bis HCl salt.

During our lead optimization efforts we were able to obtain an X-ray structure of **50** bound to Akt1. The crystal structure confirmed that the pyrrolopyrimidine core interacts via a pair of H-bonds to the hinge region of Akt1 at Ala230 and Glu228 (Fig. 3). The longer amine side chain interacts in the carbonyl-rich region with the carboxylate side chain of Glu234 (3.3 Å) and the backbone carbonyl of Glu278 (2.9 Å). The side chain carbonyl oxygen of Asn279 is ca. 3.8 Å from the amine nitrogen, and the carboxylate

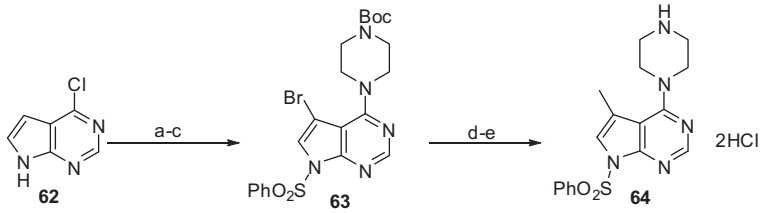


**Scheme 1.** Reagents and conditions: (a) NBS, $CDCl_3$, reflux, 79%; (b) NaH, $PhSO_2Cl$, DMF, 100%; (c) *t*-butyl piperazine-1-carboxylate, $Et_3N$, NMP, 100 °C, 86%; (d) $Me_2ZnCl$, $Pd(PPh_3)_4$, THF, reflux, 94%; (e) 4 N HCl–dioxane, DCM, 100%.

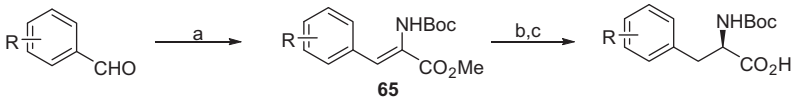


**Scheme 2.** Reagents and conditions: (a) methyl 2-(*t*-butoxycarbonyl)-2-(dimethoxyphosphoryl) acetate, tetramethylguanidine, DCM, 0 °C–rt, 2 h, 55–82%; (b) 1% Rh-(*R*,*R*)-DuPhos, MeOH:EtOAc, 40 psi $H_2$, 12 h, 88–96%; (c) LiOH, $H_2O$:THF:MeOH, 0 °C, 6 h, 90–96%, >95% ee.

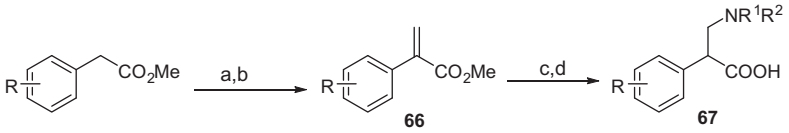


**Scheme 3.** Reagents and conditions: (a) paraformaldehyde, 10% NaOMe, DMSO, rt, 12 h, 51–98%; (b) MsCl, TEA, DCM, 0 °C–rt, 12 h, 95%; (c) $NR^1R^2$, THF, 0 °C, 12 h; $Boc_2O$, rt, 6 h, 72–91%; (d) LiOH–$H_2O$, THF/MeOH/$H_2O$, 0 °C–rt, 4 h, 86–92%.

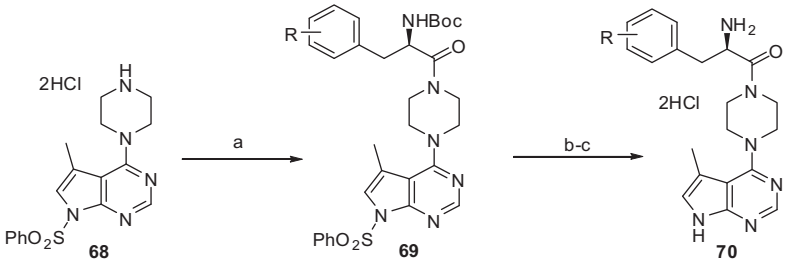


**Scheme 4.** Reagents and conditions: (a) HBTU, Hünig's base, amino acid, DCM, 4 h, 88–99%; (b) LiOH–$H_2O$, THF/MeOH/$H_2O$, 0 °C–rt, 4 h, 88–96%; (c) 4 N HCl, DCM, rt, 4 h, 92–99%.

oxygen of Asp292 is 3.5 Å. The 4-Cl phenyl group occupies a small hydrophobic pocket under the P-loop that is formed when Phe161 is displaced toward the C-helix. The 4-Cl group appears nearly ideal, given its relatively high *C* log *P* and small size.

In vitro ADME evaluation of many analogs revealed **54** as a candidate for further evaluation. Although **54** exhibited moderate cell potency (cell $IC_{50}$ = 160 nM), it also displayed low predicted clearance (3.4 mL/min/kg, human hepatocytes), and assessment of plasma protein binding in both human and mouse models suggested the potential for high free fraction (human 65%, mouse 66% bound). The Caco-2 permeability was measured for **54** at $6.8 \times 10^{-6}$ cm/s, (apical to basolateral) and $26.1 \times 10^{-6}$ cm/s for the reverse direction, (basolateral to apical). The modest asymmetry suggested some form of active efflux, most likely mediated by P-glycoprotein transporters. The solubility of **54** was excellent at greater than 50 mg/mL (at pH 6.5 and 7.4). The predicted low clearance, high free fraction, and excellent solubility properties of **54** suggested it would be suitable for use in proof-of-concept studies in human tumor mouse xenograft experiments.

The U87 human glioblastoma tumor cell line is PTEN negative and displays a high level of Akt phosphorylation.[10] U87 tumor

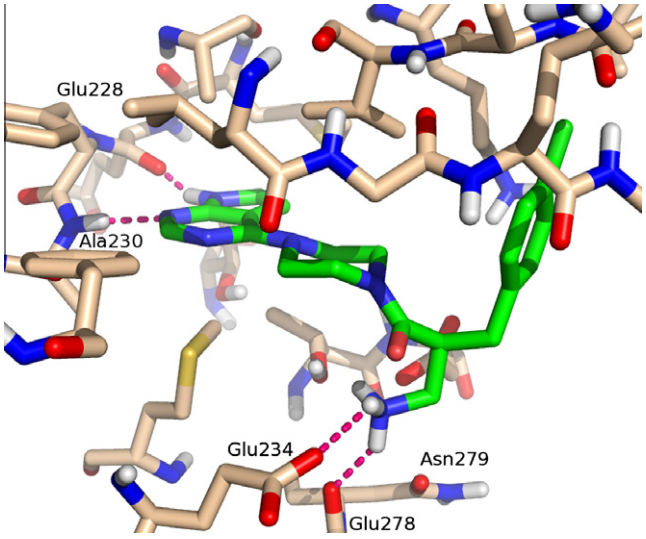


**Figure 3.** X-ray structure of **50** bound to Akt1, solved at 2.7 Å resolution (PDB code: 3OCB).[14]

xenografts implanted in female nude mice showed that p-PRAS40 levels decreased to 15% of control at 1 h (normalized to total Erk) following ip injection of 20 mg/kg **54** (Fig. 4). At 4 h, the p-PRAS40 levels were still only 40% of control, but were starting to recover. Plasma levels of **54** at 1 h were ca. 3.8 μM, and were less than 0.2 μM at 4 h, which was consistent with the observed PD effect.

Following the initial proof-of-concept results, we undertook tolerability studies in preparation for more advanced tumor growth inhibition experiments. Unfortunately, subcutaneous (sc) injection of **54** in male CD-1 mice ranging from 20 to 60 mg/kg uniformly produced death by ca. 4 h. Screening of **54** against a broad panel of kinases found the compound displayed potent inhibition versus CaMKIV, PKA, PDK1, PKC(γ, βI, η, θ), p70S6K, ROCK1, and AMPK (>90% inhibition at 1 μM).[11] To see if the poor tolerability was due to the overall pharmacophore rather than an on target effect, we evaluated **59**, a weak inhibitor (cell $IC_{50}$ = 11.8 μM) at doses ranging from 20 to 100 mg/kg, via sc injections. This compound was well tolerated, suggesting that the overall scaffold was not inherently problematic. The kinase inhibition profile of **59** showed potent inhibition of PKA, MSK1, and p70S6K (>90% inhibition at 1 μM). Interestingly, **55** (cell $IC_{50}$ = 4.2 μM) was not tolerated using the above paradigm (MTD <20 mg/kg, ip). Kinase panel screening of **55** revealed significant inhibition of PKA $IC_{50}$ = 1 nM, with MSK1, PRK2, PRKG1, PrKX, ROCK1/2, Rsk1-4, CHK2, p70S6K, and MRCKβ all showing greater than 90% inhibition at 1 μM. This suggested that some off-target activity, likely kinase-related, is the cause of the poor tolerability of these inhibitors, and that development of a selective Akt inhibitor would be better tolerated. Supporting this notion, MK-2206, which is a highly selective allosteric Akt inhibitor, is reported to be well tolerated in preclinical animal models.[12]

As documented above, the pyrrolopyrimidines tended to posses potent inhibition of undesirable kinases (i.e., ROCK1/2, PKA, etc.),[13] though a few examples did show a more selective profile. In particular, **61** showed PKA $IC_{50}$ = 278 nM, with PKA/Akt1 = 13 (Fig. 5). Interestingly, selectivity (PKA/Akt1) in this series increases from 1.2 for the 5-methyl (**46**), to 4.3 for the 6-methyl (**60**). For the quinazoline series of compounds, the PKA/Akt1 ratio tended to be ca. 7 for most analogs, though **25** showed a slightly higher ratio of 12.

All of these results suggested that increased steric bulk near the gatekeeper residue tended to improve the selectivity profile, relative to PKA. We note that PKA has a valine residue equivalent to Ala230 of Akt1; this change may allow adjustment of the gatekeeper and surrounding residues to accommodate a larger ligand in Akt1. Also, the substitution of Leu (PKA) for Met281 at the base of the hinge region tends to afford less space in PKA. Given the above profiles and tolerability issues, we decided to focus our efforts on alternative hinge binding cores that offered a better kinase selectivity profile; forthcoming papers will address these selectivity issues.

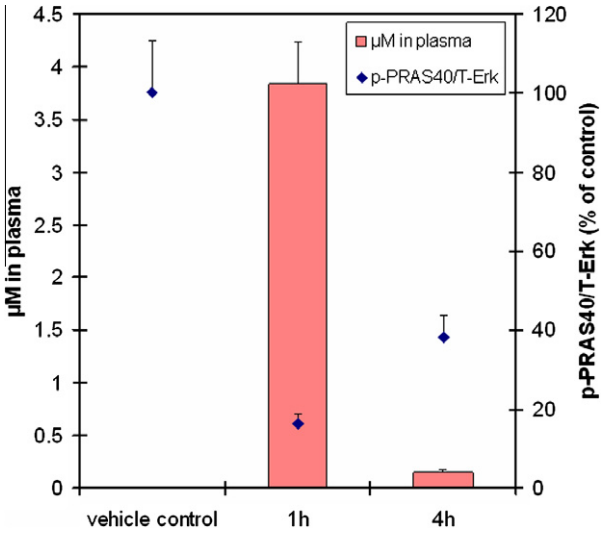


**Figure 4.** Evaluation of **54** dosed 20 mg/kg ip in the U87 human glioblastoma xenograft model, results of four experiments. p-PRAS40 is normalized to total Erk.

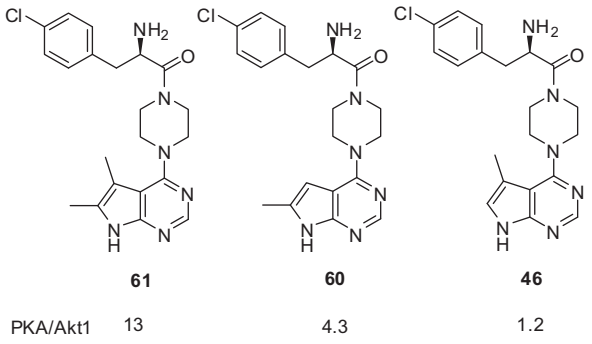


**Figure 5.** Prototype compounds with variable PKA/Akt1 selectivity. Ratio is calculated from PKA/Akt1 enzyme IC50s.

We have described the discovery and optimization of a series a pyrrolopyrimidine based pan inhibitors of Akt. The compounds display potent enzyme and cell based inhibition of our primary targets Akt1/2/3. Additionally, the compounds display excellent knockdown of p-PRAS40 in tumor xenografts, combined with high solubility and good ADME properties. While this profile is encouraging, the lack of selectivity against related kinases, in particular PKA and ROCK1/2 render them poorly tolerated and unsuitable for development as therapeutic agents.

## Supplementary data

Supplementary data associated with this article can be found, in the online version, at doi:10.1016/j.bmcl.2010.08.053.

## References and notes

1. Cheng, J. Q.; Lindsley, C. W.; Cheng, G. Z.; Yang, H.; Nicosia, S. V. *Oncogene* **2005**, *24*, 7482.
2. Altomare, D. A.; Testa, J. R. *Oncogene* **2005**, *24*, 7455.
3. Lian, Z.; Di Cristofano, A. *Oncogene* **2005**, *24*, 7394; Chen, Y. L.; Law, P.-Y.; Loh, H. H. *Curr. Med. Chem. Anticancer Agents* **2005**, *5*, 575; Lu, Y.; Wang, H.; Mills, G. B. *Rev. Clin. Exp. Hematol.* **2003**, *7*, 205; Mitsiades, C. S.; Mitsiades, N.; Koutsilieris, M.; Nicholson, K. M.; Anderson, N. G.; Neri, L. M.; Borgatti, P.; Capitani, S.; Martelli, M.; Brazil, D. P.; Hemmings, B. A. *Curr. Cancer Drug Targets* **2004**, *4*, 235.
4. Masure, S.; Haefner, B.; Wesselink, J. J.; Hoefnagel, E.; Mortier, E.; Verhasselt, P.; Tuytelaars, A.; Gordon, R.; Richardson, A. *Eur. J. Biochem.* **1999**, *265*, 353.
5. Degtyarev, M.; De Mazière, A.; Orr, C.; Lin, J.; Lee, B. B.; Tien, J. Y.; Prior, W. W.; van Dijk, S.; Wu, H.; Gray, D. C.; Davis, D. P.; Stern, H. M.; Murray, L. J.; Hoeflich, K. P.; Klumperman, J.; Friedman, L. S.; Lin, K. *J. Cell Biol.* **2008**, *183*, 101.
6. Inhibition of Akt1, Akt2, Akt3, and PKA was determined using the IMAP format. A detailed description of the assay format is provided in the Supplementary data.
7. PDB Code 1O6K: Yang, J.; Cron, P.; Good, V. M.; Thompson, V.; Hemmings, B. A.; Barford, D. *Nat. Struct. Biol.* **2002**, *9*, 940.
8. Docking studies were performed using the Glide program (Glide V4.5; Schrödinger, L.L.C.: New York, NY, 2005) Friesner, R. A.; Banks, J. L.; Murphy, R. B.; Halgren, T. A.; Klicic, J. J.; Mainz, D. T.; Repasky, M. P.; Knoll, E. H.; Shelley, M.; Perry, J. K.; Shaw, D. E.; Francis, P.; Shenkin, P. S. *J. Med. Chem.* **2004**, *47*, 1739.
9. The cell-based assay monitored the phosphorylation of Thr246 on PRAS40 in LNCaP cells. A detailed description of the assay format is provided in the Supplementary data.
10. Wen, S.; Stolarov, J.; Myers, M. P.; Su, J. D.; Wigler, M. H.; Tonks, N. K.; Durden, D. L. *Proc. Natl. Acad. Sci.* **2001**, *98*, 4622.
11. The inhibition against a panel of kinases was determined at Upstate, Charlottesville, VA (256 total kinases screened).

12. Hirai, H.; Sootome, H.; Nakatsuru, Y.; Miyama, K.; Taguchi, S.; Tsujioka, K.; Ueno, Y.; Hatch, H.; Majumder, P. K.; Pan, B. S.; Kotani, H. *Mol. Cancer Ther.* **2010**, *9*, 1956.
13. Reiken, S.; Lacampagne, A.; Zhou, H.; Kherani, A.; Lehnart, S. E.; Ward, C.; Haung, F.; Gaburjakova, M.; Gaburjakova, N.; Rosemblit, N.; Warren, M. S.; He, K.; Yi, G.; Wang, J.; Burkhoff, D.; Vassort, G.; Marks, A. R. *J. Cell Biol.* **2003**, *160*, 919; Doe, C.; Bentley, R.; Behm, D. J.; Lafferty, R.; Stavenger, R.; Jung, D.; Bamford, M.; Panchal, T.; Grygielko, E.; Wright, L. L.; Smith, G. K.; Chen, Z.; Webb, C.; Khandekar, S.; Yi, T.; Kirkpatrick, R.; Dul, E.; Jolivette, L.; Marino, J. P., Jr.; Willette, R.; Lee, D.; Hu, E. *J. Pharmacol. Exp. Ther.* **2007**, *320*, 89.
14. Atomic coordinates of the structure **50** bound to Akt1 were deposited with the RCSB Protein Data Bank (PDB) under the accession code 3OCB.